Supporting Information for:

Elucidating the Particle Size-Dependent Guest-Induced Structural Transition of Flexible Metal–Organic Frameworks by Exploring Cooperative Nature

Homare Arima,[a] Shotaro Hiraide,*[a] Satoshi Watanabe*[a]

[a] *Department of Chemical Engineering, Kyoto University, Nishikyo, Kyoto 615-8510, Japan.*
E-mail: hiraide@cheme.kyoto-u.ac.jp, nabe@cheme.kyoto-u.ac.jp

Contents

S1. Derivation of eqn 12

Differential free energy , μ, is calculated as

$$\begin{aligned}\mu(m,P) &= \frac{\partial \Delta\Omega_{\mathrm{os}}}{\partial m} \\ &= \Delta\Omega_{\mathrm{os}}(m+1,P) - \Delta\Omega_{\mathrm{os}}(m,P) \\ &= -k_{\mathrm{B}}T \ln \frac{1}{(m+1)!} \sum_{\boldsymbol{r}^{m+1}} \exp\left(-\frac{E(\boldsymbol{r}^{m+1},P)}{k_{\mathrm{B}}T}\right) + k_{\mathrm{B}}T \ln \frac{1}{m!} \sum_{\boldsymbol{r}^{m}} \exp\left(-\frac{E(\boldsymbol{r}^{m},P)}{k_{\mathrm{B}}T}\right) \\ &= -k_{\mathrm{B}}T \ln \frac{1}{m+1} \frac{\sum_{\boldsymbol{r}^{m+1}} \exp(-E(\boldsymbol{r}^{m+1},P)/k_{\mathrm{B}}T)}{\sum_{\boldsymbol{r}^{m}} \exp(-E(\boldsymbol{r}^{m},P)/k_{\mathrm{B}}T)}\end{aligned} \tag{1}$$

where $\boldsymbol{r}^m = (\boldsymbol{r}_1, \boldsymbol{r}_2, ..., \boldsymbol{r}_m)$ and $\sum_{\boldsymbol{r}^m} = \sum_{\boldsymbol{r}_1}\sum_{\boldsymbol{r}_2}...\sum_{\boldsymbol{r}_m}$. Defining the energy that the op cell with $\boldsymbol{r}_{m+1}$ receives from the other op cells as E^+,

$$E(\boldsymbol{r}^{m+1},P) = E(\boldsymbol{r}^{m},P) + E^{+}(\boldsymbol{r}_{m+1};\boldsymbol{r}^{m},P) \tag{2}$$

is obtained. Notably,

$$E(\boldsymbol{r}^{m},P) = m\Delta\omega_{\mathrm{os}}^{\mathrm{op}} + E_{\mathrm{IUC}}(\boldsymbol{r}^{m},P) \tag{3}$$

and thus,

$$E^{+}(\boldsymbol{r}_{m+1};\boldsymbol{r}^{m},P) = \Delta\omega_{\mathrm{os}}^{\mathrm{op}} + E_{\mathrm{IUC}}^{+}(\boldsymbol{r}_{m+1};\boldsymbol{r}^{m},P) \tag{4}$$

where E_{IUC}^{+} is the total inter-unit-cell interaction that the op cell with $\boldsymbol{r}_{m+1}$ receives. Here, considering the summation of the exponential of energy,

$$\begin{aligned}\sum_{\boldsymbol{r}^{m+1}} \exp\left(-\frac{E(\boldsymbol{r}^{m+1},P)}{k_{\mathrm{B}}T}\right) &= \sum_{\boldsymbol{r}_1}...\sum_{\boldsymbol{r}_m}\sum_{\boldsymbol{r}_{m+1}} \exp\left(-\frac{E^{+}(\boldsymbol{r}_{m+1};\boldsymbol{r}^{m},P)}{k_{\mathrm{B}}T}\right)\exp\left(-\frac{E(\boldsymbol{r}^{m},P)}{k_{\mathrm{B}}T}\right) \\ &= \sum_{\boldsymbol{r}_{m+1}}\left\{\sum_{\boldsymbol{r}^{m}} \exp\left(-\frac{E^{+}(\boldsymbol{r}_{m+1};\boldsymbol{r}^{m},P)}{k_{\mathrm{B}}T}\right)\exp\left(-\frac{E(\boldsymbol{r}^{m},P)}{k_{\mathrm{B}}T}\right)\right\} \\ &\equiv \sum_{\boldsymbol{r}_{m+1}} A(\boldsymbol{r}_{m+1};\boldsymbol{r}^{m},P)\end{aligned} \tag{5}$$

is introduced. As the meaning of A is the summation over all the state in $\boldsymbol{r}^m$ under the periodic boundary conditions, the A value is the same regardless of $\boldsymbol{r}_{m+1}$; thus,

$$\sum_{\boldsymbol{r}^{m+1}} \exp\left(-\frac{E(\boldsymbol{r}^{m+1},P)}{k_{\mathrm{B}}T}\right) = M\sum_{\boldsymbol{r}^{m}} \exp\left(-\frac{E^{+}(\boldsymbol{r}_{m+1};\boldsymbol{r}^{m},P)}{k_{\mathrm{B}}T}\right)\exp\left(-\frac{E(\boldsymbol{r}^{m},P)}{k_{\mathrm{B}}T}\right) \tag{6}$$

Substituting the equation into eqn 1 of this section yields:

$$\mu(m,P) = -k_{\mathrm{B}}T \ln\left\{\frac{M}{m+1} \times \frac{\sum_{\boldsymbol{r}^{m}} \exp(-E(\boldsymbol{r}^{m},P)/k_{\mathrm{B}}T)\exp(-E^{+}(\boldsymbol{r}^{m},P)/k_{\mathrm{B}}T)}{\sum_{\boldsymbol{r}^{m}} \exp(-E(\boldsymbol{r}^{m},P)/k_{\mathrm{B}}T)}\right\} \tag{7}$$

where the last term in the $\{\}$ cabinet is the ensemble average of a term relating to the energy received when an additional op cell is inserted into a system, E^+. Therefore, eqn 12 in the main paper is introduced.

S2. Particle size distribution for the ELM-11 samples

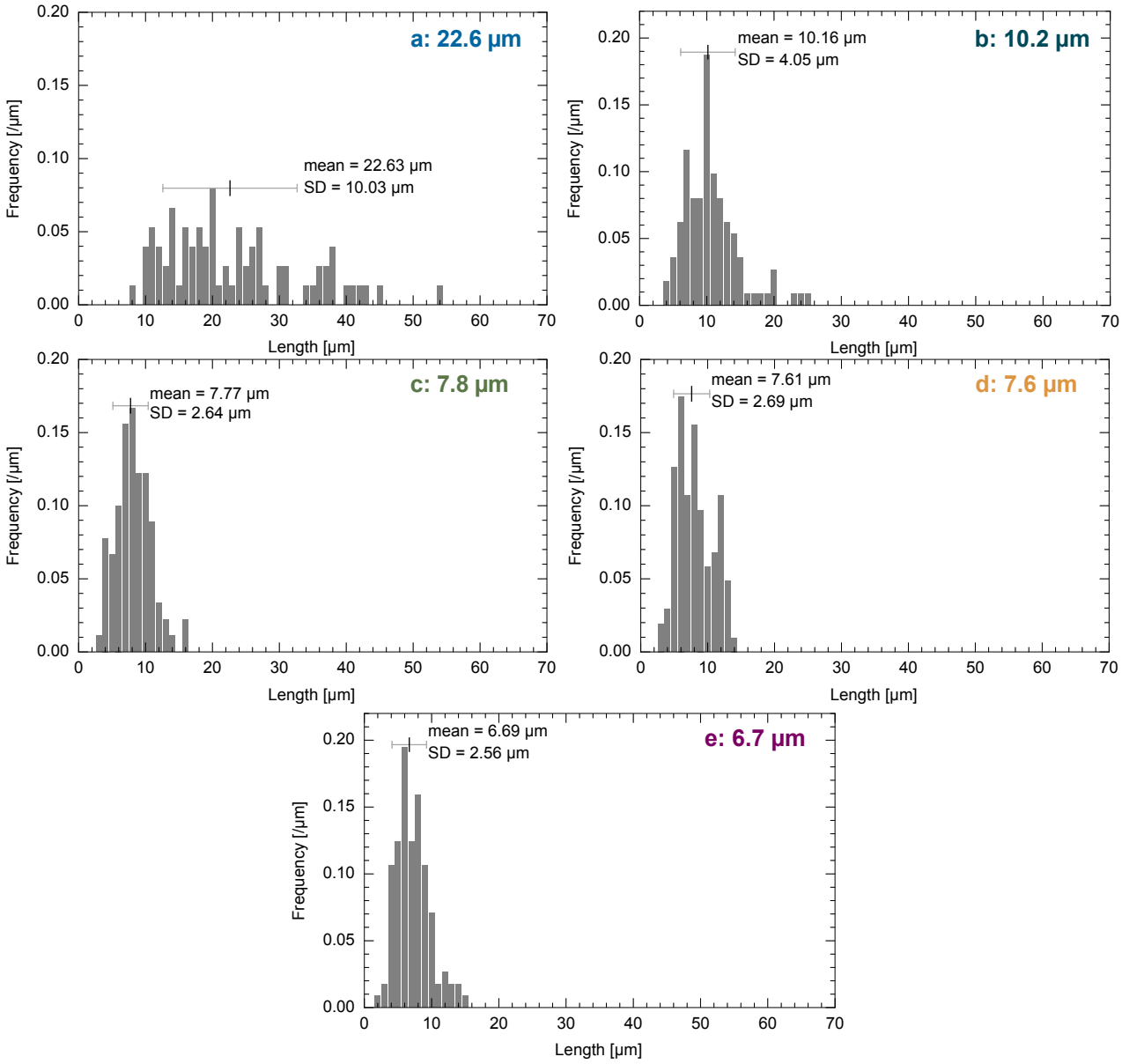

Fig. S1 Particle size distribution of the synthesized ELM-11.

S3. Explanation of particle-size dependence based on the primitive theory and its shortcomings

The nanoscale simulation was conducted on the simplified model having $10\sigma_{gg} \times 10\sigma_{gg}$ layers. This model cannot show the particle-size dependence which agrees with experimental observations. When the layers measure $30\sigma_{gg} \times 30\sigma_{gg}$, this layer can be regarded as nine of the small layers ($10\sigma_{gg} \times 10\sigma_{gg}$) which undergo transition simultaneously; that is, free energy scales linearly with layer size, nine times in this case. Assuming that the thermal fluctuation does not depend on layer size, hysteresis loop expands because energy barriers scale also linearly with layer size (Fig. S2). Even if the thermal fluctuation were proportional to layer size, the hysteresis width of larger particles would be the same, but not narrower.

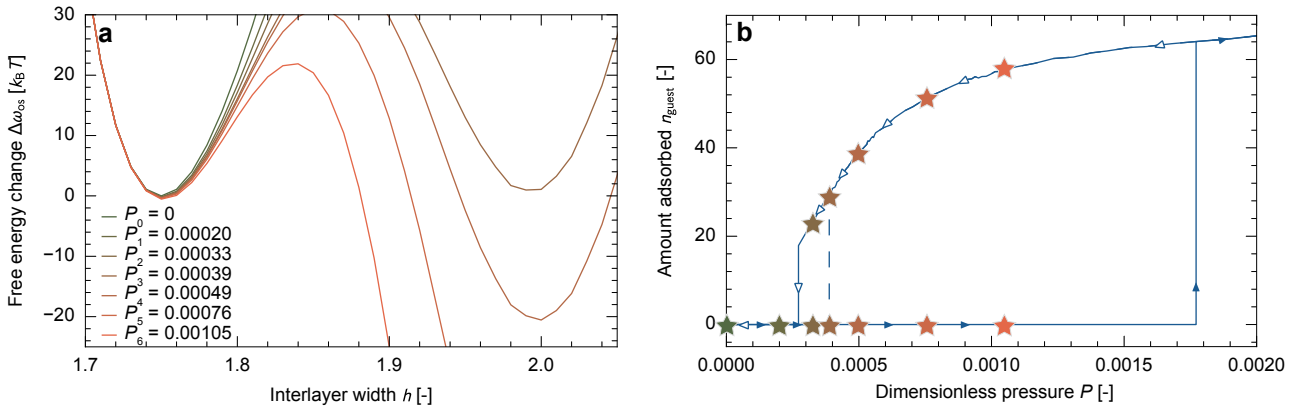

Fig. S2 (a) Free energy profiles of the unit-cell ($30\sigma_{gg} \times 30\sigma_{gg} \times h$) at various pressures. (b) Adsorption isotherms of the unit-cell. The transition from cp to op states occurs thermodynamically at the same pressure as $10\sigma_{gg} \times 10\sigma_{gg}$ model, but the hysteresis loop expands: the adsorption pressure increases and the desorption one decreases (solid line).

S4. Downward-convex profile inducing a gradual increase in the amount adsorbed

When free energy profiles show a downward convex, the stable states where the $\Delta\Omega_{os}$ values reach the minimum shift gradually in response to pressure change. In this model, the amount adsorbed is roughly proportional to the number of op cells, so a gradual increase in the amount adsorbed occurs due to a gradual change in stable states.

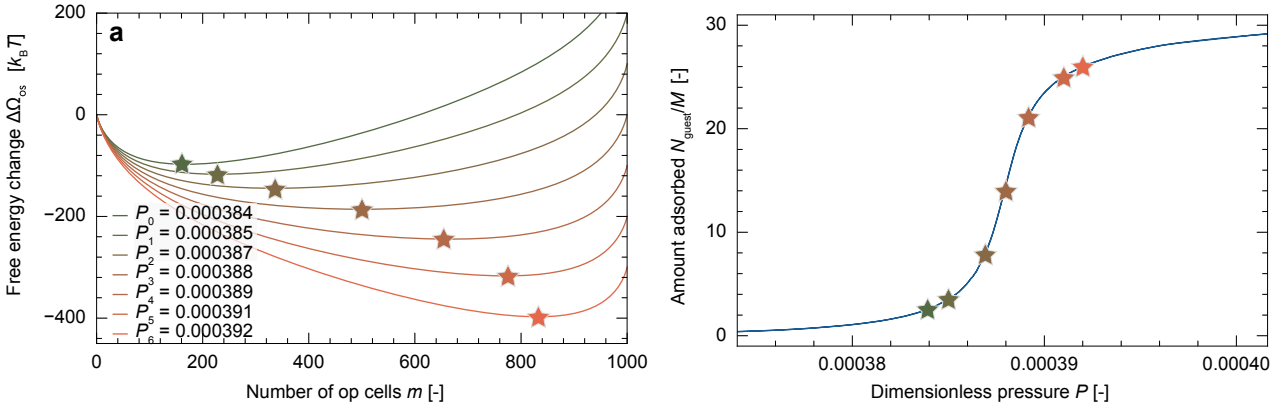

Fig. S3 (a) Free energy profiles of the particle model with a weak interaction parameter, $J_{\#} = 0.6k_BT$, at various pressures. (b) Adsorption isotherms for the particle. A gradual change in stable states causes a gradual increase in the amount adsorbed.

S5. Particle-thickness dependence

Fig. S4 depicts adsorption isotherms with various M_z, where $M_\# = 10$ and $J_z = 0$. All simulated isotherms presented below were obtained by averaging 10 separate simulations to obtain smooth profiles. Although particle size in the x- and y-directions contributed to changing the transition behaviors, the particle thickness did not so. In this $J_z = 0$ condition, the number of stacked layers did not matter because neighboring cells in different states in the z-direction incurred no energetic penalty to affect the free energy profiles.

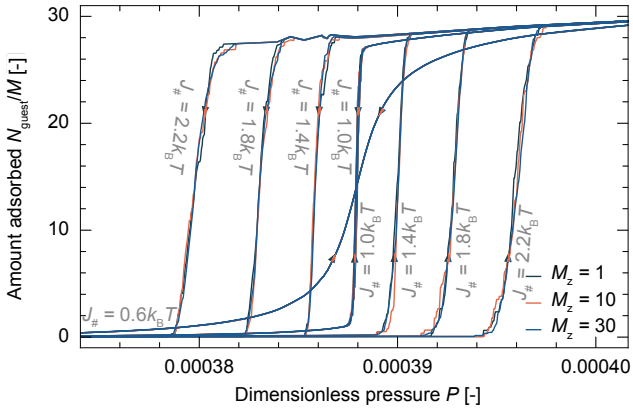

Fig. S4 Adsorption isotherms for the particle models with various M_z when $M_\# = 10$. With any $J_\#$ values, the adsorption behaviors were not changed by M_z.

S6. Simulated adsorption isotherms with various $M_{\#}$

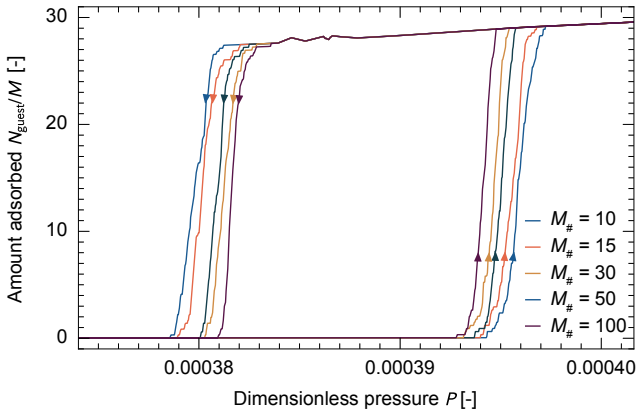

Fig. S5 Adsorption isotherms for the particle model with the different numbers of unit cells in the x- or y-directions, $M_{\#}$, when $M_z = 10, J_{\#} = 2.2k_{\mathrm{B}}T$, and $J_z = 0$.

S7. Determination of the equilibrium transition pressure

The $\Delta\omega_{os}^{op}$ values at the gate adsorption and desorption pressures are the same absolute value with an opposite sign (eqn 19). The free energy change can be calculated by thermodynamic integration for adsorption isotherms, which is equal to the area of adsorption isotherm when the x-axis is chemical potential (or $\log P$). Therefore, dividing the area between P_{ads} and P_{des} into two equal parts would enable obtaining the equilibrium pressure, P_{eq} (Fig. S6a). Strictly speaking, the $\Delta\omega_{os}^{op}$ value should be obtained by integrating n_{guest}^{op}, which is usually estimated by fitting an isotherm with a Langmuir plot or another appropriate fitting method[1]. That is, the integration including the intermediate part of the S-shaped curve does not give the correct $\Delta\omega_{os}^{op}$ values. However, the proposed method would provide a good approximation because the non-integrated areas for the adsorption branch is almost the same as that for the desorption branch. By conducting the proposed method for our experimental results (Fig. 2g), the P_{eq} values were calculated for each sample (Fig. S6b), where these transition pressures, P_{ads} and P_{des}, were defined as pressures at half maximum uptake[2]. The results showed equilibrium pressures at 29.01 kPa with a vibration range of $\pm$0.4 kPa, while the adsorption and desorption pressures varied by approximately 2 kPa. In conclusion, we successfully developed the P_{eq} determination method and led the equilibrium transition pressure of the CO_2 adsorption on ELM-11 at 273 K.

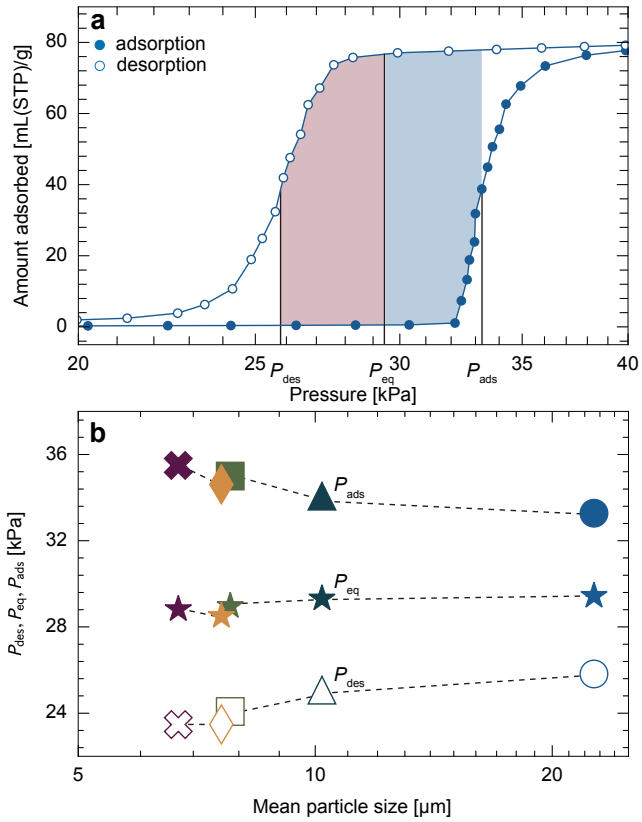

Fig. S6 (a) Illustration for estimating P_{eq} by dividing the area into two equal parts, whose x-axis is a log scale. (b) The obtained P_{eq}, P_{ads}, and P_{des} values with various particle sizes. Although the kinetic transition pressures, P_{ads} and P_{des}, change, the equilibrium transition pressure, P_{eq}, seems constant. These analyses were performed on Fig. 2g.

S8. Cooperative transition behavior under various conditions

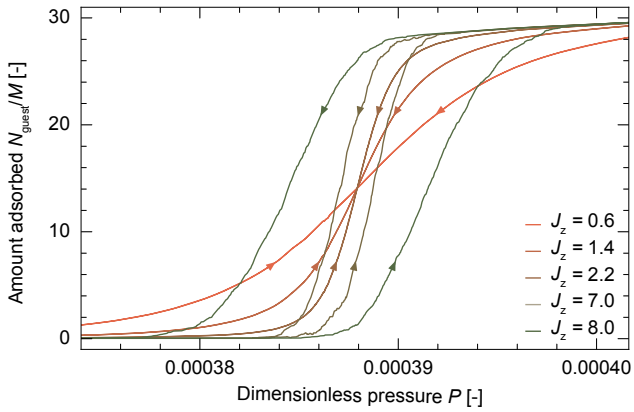

Fig. S7 Adsorption isotherms for the particle models with various J_z under $J_\# = 0, M_\# = 10$, and $M_z = 10$, which showed less distinct S-shapes than the typical condition

The DUT-8(Ni) systems reportedly exhibit an anisotropic size effect[2]. DUT-8 has a stronger connection in the c-axis, resulting in a rod-like shaped particle. However, the size effect is weaker thorough the direction, which is contrary to intuition. The strange anisotropic size dependence was expressed by the particle model with the $J_\#(= 1.4k_BT)$ value which is a bit smaller than $J_z(= 2.2k_BT)$ (Fig. S8). Fig. S8a depicts adsorption isotherms on the particle with various $M_\#$ and the constant M_z, which shows the size effect of $M_\#$. Fig. S8b depicts adsorption isotherms on the particle with constant $M_\#$ and the various M_z, which shows no obvious size effects of M_z.

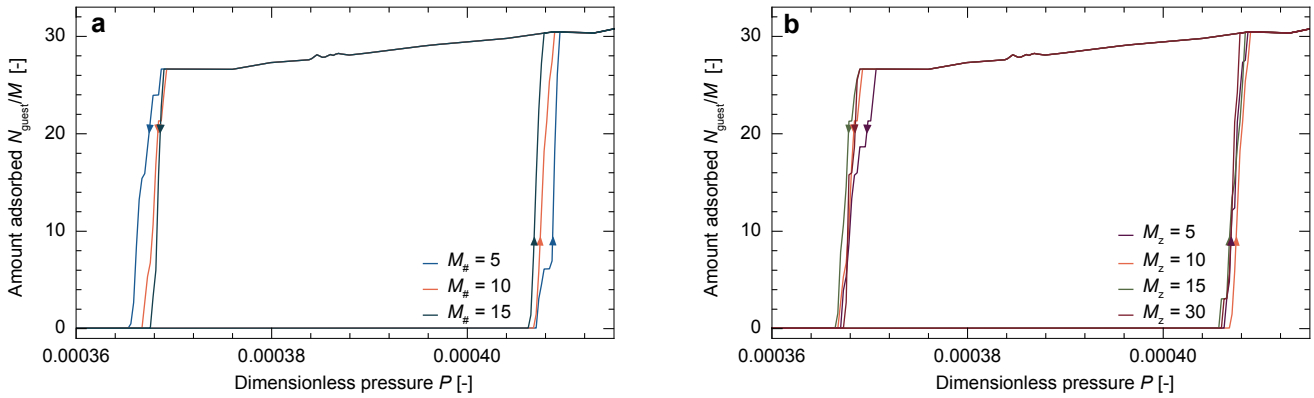

Fig. S8 (a) Adsorption isotherms for the particle with various $M_\#$ and the constant M_z and (b) with the constant $M_\#$ and various M_z, where $J_\# = 1.4k_BT$ and $J_z = 2.2k_BT$.

Isotropic three-dimensional solid–solid interaction can be also discussed. The principle of causing particle size dependence is completely the same as two-dimensional interactions. Because the interfacial penalty occurs between not only in the x- and y- directions but also in the z-direction, the transition state forms as a cubic shape to minimize interface area in the initial stage, referred in Fig. 5a, as shown in Fig. S9. The adsorption isotherms changed depending on the particle size, in particular, the number of cells in the model, though changing the aspect ratio did not cause a great effect on hysteresis behavior.

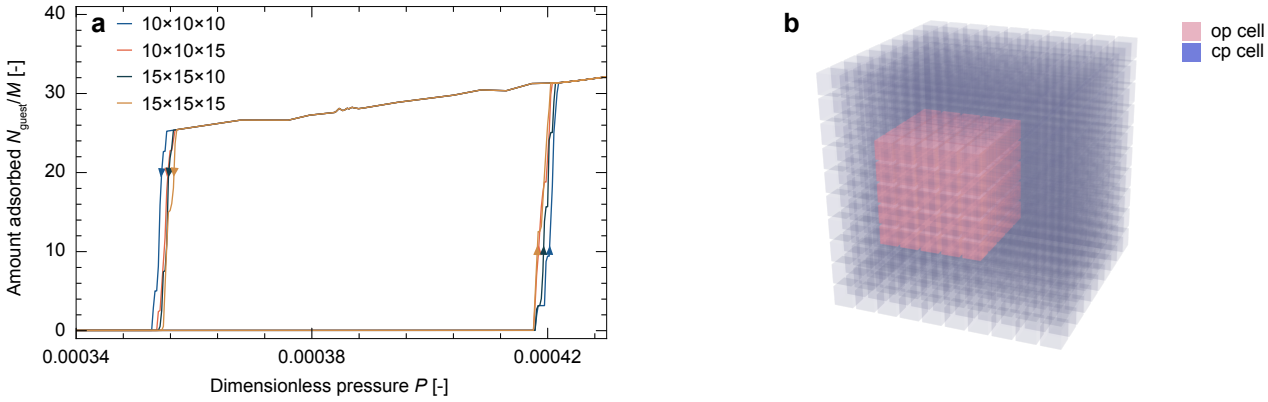

Fig. S9 (a) Adsorption isotherms for the particle model with the different size and $J_{\#} = J_z = 2.2k_{\mathrm{B}}T$ and (b) a transition state of the model measuring $M_x \times M_y \times M_z = 10 \times 10 \times 10$ with three-dimensional interaction.

S9. Details of the nanoscale simulation

The nanoscale simulation was conducted on a simplified unit-cell model developed in our previous study[3]. The complete details are found in[3–5]. The structure of stack-layered MOFs, such as ELM-11, was simplified to obtain free energy profiles. This model comprised a rigid smeared-carbon wall and single atoms (Ar) mimicking the square-grid layer and organic pillars Fig. S10. A simulation box was composed of seven unit-cells, which measured $10\sigma_{gg} \times 10\sigma_{gg} \times h$ where σ_{gg} is a size parameter of the Lennard-Jones potential for guest molecules (Ar) and h is interlayer width. Grand canonical Monte Carlo simulation was performed with various interlayer widths ($1.70\sigma_{gg}$–$2.05\sigma_{gg}$) in steps of $0.01\sigma_{gg}$ to obtain the amount adsorbed on simulation boxes, n_{guest}.

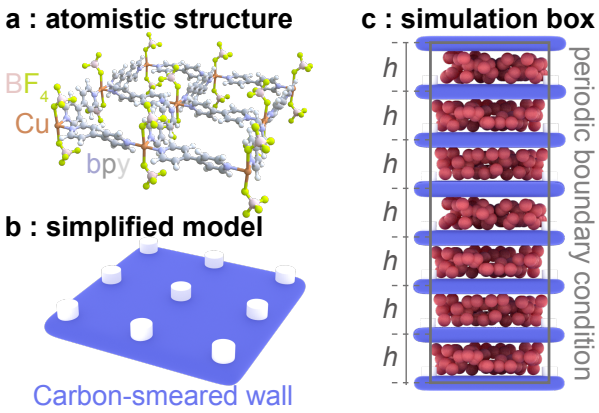

Fig. S10 (a) The atomistic model of an ELM-11 layer and (b) the simplified layer model of the ELM-11 structure. (c) Simulation box consisting of the stacked seven layers.

References

1 F.-X. Coudert, M. Jeffroy, A. H. Fuchs, A. Boutin and C. Mellot-Draznieks, *J. Am. Chem. Soc.*, 2008, **130**, 14294–14302.

2 L. Abylganzia, I. Senkovska, R. Engemann, S. Ehrling, T. E. Gorelik, N. Kavoosi, U. Kaiser and S. Kaskel, *Front. Chem.*, 2021, **9**, 674566.

3 R. Numaguchi, H. Tanaka, S. Watanabe and M. T. Miyahara, *J. Chem. Phys.*, 2013, **138**, 054708.

4 S. Hiraide, H. Arima, H. Tanaka and M. T. Miyahara, *ACS Appl. Mater. Interfaces*, 2021, **13**, 30213–30223.

5 H. Arima, S. Hiraide, M. T. Miyahara and S. Watanabe, *ACS Appl. Mater. Interfaces*, 2023, **15**, 36975–36987.